Error Bounds for MEG and EEG Source Localization

John C. Mosher,*† Michael E. Spencer,*# Richard M. Leahy,* and Paul S. Lewis†

*Signal & Image Processing Institute, University of Southern California, Los Angeles, CA 90089-2564
†Los Alamos National Laboratory, MEE-3 MS J580, Los Alamos, NM 85745
#TRW Space and Defense, One Space Park, Redondo Beach, CA 90278

Abstract

Localization error bounds are presented for both EEG and MEG as graphical error contours for a 37 sensor arrangement. Both one and two dipole cases were examined for all possible dipole orientations and locations within a head quadrant. The results show a strong dependence on absolute dipole location and orientation. The results also show that fusion of the EEG and MEG measurements into a combined model reduces the lower bound. A Monte-Carlo simulation was performed to check the tightness of the bounds for a selected case. The simple head model, the white and relatively low power noise, and the few relatively strong dipoles were all selected in this study as optimistic conditions to establish possibly fundamental resolution limits for any localization effort.

1.0 Introduction

Electroencephalograms (EEG) and magnetoencephalograms (MEG) are non-invasive methods of studying the functional activity of the human brain with millisecond temporal resolution. Much of the work in EEG and MEG in the last few decades has been focused on estimating the properties of the internal localized sources of the fields from the external measurements. The most straightforward model for describing the surface evoked potential or the external evoked magnetic field is the single equivalent current dipole. In [10], we reviewed the many variations of this dipole model and its extensions to multiple dipoles and time epochs. Each of the models, both in EEG and MEG, contains a transfer function or lead field model to relate each dipole's intensity, orientation, and location to the externally measured fields. The general inverse problem is to find the three location parameters and the three moment parameters that comprise the unknown parameters for each dipole.

The simplest head model in use is a set of homogeneous spherical shells, for which the MEG model is straightforward and the EEG model is still tractable. Although a dipole comprises six parameters, the focus of most research has been on the accuracy of determining the three location parameters. Direct analysis of the localization error is complicated by the nonlinearity of the location parameters, the sensitivity to the moment orientation, the moment intensity, the background noise power, the orientation and spatial extent of the sensors, and the absolute position of the dipole. Consequently, most studies and comparisons were restricted to specialized dipole locations or sensor positions. The error results were generally established by experimental data or by Monte Carlo analysis. More recently, dipoles implanted in patients have been used in an attempt to determine localization errors in MEG [3] and to compare localization errors between EEG and MEG [5]. The results of [5] have particularly lead to recent controversy, with the study criticized on methodological grounds in [8],[18].

Our analysis of dipole localization error for MEG and EEG is based on the well-known Cramer-Rao Lower Bound (CRLB). The CRLB provides a lower bound on the variance of any unbiased estimator of the location and other model parameters. By deriving a closed-form expression for the bound, we can compute it efficiently for a much wider range of conditions than can studies based on Monte-Carlo simulations or experimental data. The bounds are useful only if they are relatively tight (i.e. if they are not overly optimistic compared with the true localization error variances) and if the estimators employed have relatively small biases. To demonstrate the usefulness of the bounds, we present a Monte Carlo simulation which indicates that the CRLBs, in most cases of interest, give reasonably accurate predictions of actual localization error variances. Preliminary results of this analysis are presented in [9], and a more comprehensive analysis with more array configurations will be presented in [11].

The CRLB gives surprisingly large lower bounds, even under fairly optimistic assumptions. Since modeling errors

This work was supported by the Los Alamos National Laboratory, operated by the University of California for the United States Department of Energy under contract W-7405-ENG-36, by the TRW Doctoral Fellowship Program, and by the Kaprielian Innovative Research Fund at the University of Southern California. Correspondence to: Dr. R. Leahy, Signal & Image Processing Institute, University of Southern California, Los Angeles, CA 90089-2564.

1058-6393/92 $03.00 © 1992 IEEE

tend to degrade, rather than improve, performance, these results indicate that the accuracy of dipole localization based on single time epochs is often limited by the inherent ill-posed nature of the problem. The models used here are some of the simplest in use. In general, more complicated models would be more prone to modeling errors and could have more parameters to estimate. Consequently, the bounds presented here may pose fundamental limits on EEG and MEG localization performance.

2.0 Forward Models

By the superposition of electromagnetic sources, we can always separate the intensity of the sources as a linear term, whether we are considering these simple EEG and MEG spherical models or any other combination of head and source model. The vector of measured samples at time j can be modeled as

$$A(j) = \left[G(l_1)\ G(l_2)\ \ldots\ G(l_p)\right]\begin{bmatrix} q_1 \\ q_2 \\ \ldots \\ q_p \end{bmatrix}$$

$$= G(l)\,q(j) \qquad (EQ\ 1)$$

where $A(j)$ represents the general column vector of surface potential or magnetic field measurements, or a combination of both. Column vectors l and q are both concatenations of the parameters for p dipoles,

$$l = \left[l_1, \ldots, l_p\right]^T \text{ and } q = \left[q_1, \ldots, q_p\right]^T.$$

The vector l_i represents the three-dimensional location of the ith current dipole, and q_i represents the corresponding three-dimensional dipole moment. $G(l_i)$ represents the "gain transfer" matrix for the ith dipole, which relates the dipoles' moments to the vector of measurements and has a nonlinear dependence on the dipole locations.

2.1 Four Concentric Sphere Model for EEG

The EEG dipole model is the more complex of the two models, and assumptions must be made for the conductivities and shell thicknesses. In this paper we use the four concentric sphere model. For a single dipole model at point l_i, each element in (1) of the column vector of surface potential measurements represents the voltage at a single surface point p and is expressed as the inner product of the (3 x 1) gain vector g_v and the (3 x 1) dipole moment vector q:

$$V(p) = g_v^T(l_i, p)\,q \qquad (EQ\ 2)$$

where for clarity we show the dependence of the gain vector on both the dipole location and sensor position. The gain matrix $G(l)$ for a single dipole is the concatenation of the gain vectors for all sensor positions p.

For a dipole on the z-axis, the potential on the surface of the four sphere model referenced to infinity is derived in [6]. In [11],[13], we extend this rather lengthy formula for other dipole locations by applying rotation transformations to the basic formulas. The form of (2) explicitly shows that the voltage has a nonlinear dependence on the dipole and electrode locations and a linear dependence on the dipole moment.

Fig. 1 shows the four spheres with their respective radii and conductivities. Overlaid on the spheres are the sensor locations for the 37 channel pattern. The conductivities and radii shown were taken from [6]. We note that the relatively thin skull thickness, 4 mm in this case, gives favorable values for dipole localization; thicker skulls will produce higher error bounds.

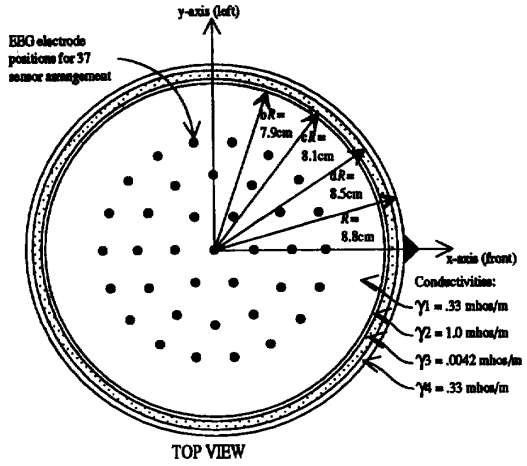

FIGURE 1. Arrangement for 37 sensors over the surface of the head.

2.2 Biot-Savart Law for MEG

Compared with its EEG counterpart, the MEG model for the dipole in a sphere with radially oriented sensors is quite simple. Radially oriented dipoles produce no magnetic field outside the concentric conducting spheres, regardless of the number of spheres we consider, and return volume currents produce no external magnetic fields in the radial direction. Sarvas [12] provides a thorough derivation of the general MEG formulas, then presents the simplifications that result for the spherically symmetric head model with radially oriented sensors.

For radially oriented sensors, the measured field is a relatively simple function of only the tangential components of the dipole moments. We restrict ourselves to the radially oriented sensors, primarily for simplicity in presentation.

This model has been extensively reviewed and published in the recent literature, and we present only a brief summary to clarify the terminology in relation to our model. The radially oriented MEG sensor coil is assumed to make a point measurement of the radial magnetic field. For a dipole located at l_i, the scalar radial magnetic field $B(p)$ can be expressed as the inner product of gain vector g_B and the dipole moment q,

$$B(p) = g_B^T(l_i, p)\, q \ , \qquad (EQ\ 3)$$

for sensor coil location p. For the case of the spherical head model and the radial sensor measurements, this gain vector is a special case of the Biot-Savart law and can be expressed as

$$g_B^T(l_i, p) = \left(\frac{\mu_0}{4\pi}\right) \frac{r \times l}{\|p - l\|^3} \qquad (EQ\ 4)$$

where the coordinate system is assumed to be head centered, r is the unit radial orientation of the sensor coil, μ_0 is the permeability of free space, and " $\times$ " denotes the vector cross product. The MEG gain matrix $G(l_i)$ for a single dipole is the concatenation of all gain vectors for all sensor locations.

3.0 Cramer-Rao Lower Bounds

We follow a formulation similar to [14], with the exception that our data is real and with the enhancement that our manifold is multidimensional. We define D as the partials of the gain matrix with respect to the location parameters, and we arrange the p moments at the jth time slice into a block diagonal matrix,

$$X(j) \equiv \begin{bmatrix} I_3 \otimes q_1(j) & & 0 \\ & \cdots & \\ 0 & & I_3 \otimes q_p(j) \end{bmatrix} . \qquad (EQ\ 5)$$

We then form the Fisher Information Matrix, analytically invert, and extract the lower bound formulas for the location parameters, paralleling the work of [14]. In [9], [11], we more explicitly detail the steps, but space restricts us here to state only the result for a single time slice and equal intensity dipoles,

$$\mathrm{CRLB}(l) = \frac{\nu}{Q^2} \left[(DX_n)^T P_G^{\perp} (DX_n) \right]^{-1} , \qquad (EQ\ 6)$$

where all moments in X_n have been scaled to unity ("normalized") and their common intensity of Q brought outside the matrix.

This lower bound is a function of both the dipole's location and its orientation. Since this study restricted the dipoles to the tangential plane, we need only consider the single parameter θ that denotes the relative angle of the dipole in this plane. At each location of interest, we "scan" the dipole over all possible orientations, searching for the best and worst orientations, as well as recording the average lower bound over all angles.

Fig. 2 presents such a scan for two different array cases. The "dense" array case represents a dipole near the edge of a spatially limited array, and the "upper hemisphere" array case represents a dipole in the middle of an extensive array. We see a strong dependency on the dipole orientation for one situation and relatively little dependency for the other. We retain three values from these curves: the best (lowest) RMS error, the worst, and the average over all angles.

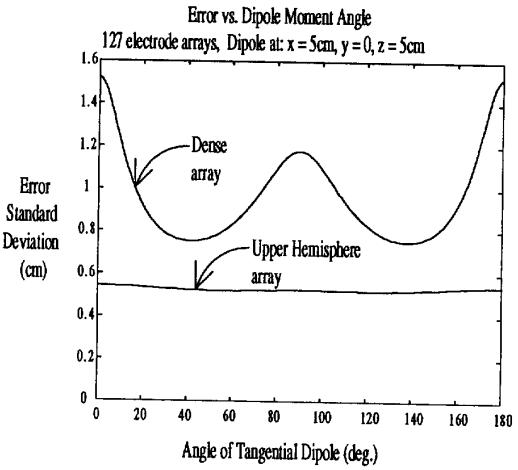

FIGURE 2. Error lower bound as a function of the angle the dipole makes in the tangential plane, for two different array cases.

4.0 EEG and MEG Analysis Example

Fig. 1 displays the array patterns used here with relation to the spherical model. The pattern is symmetric about the z-axis, which runs through the center of the array. Because of this high degree of symmetry, we restrict our analysis region to the positive x-z plane. The error results in this plane can then be inferred by symmetry for the entire upper hemisphere.

To set the dipole intensity at a physically plausible level, we reviewed other experimental and phantom studies. In [4], a relatively strong dipole was estimated to have a dipole intensity of 2.1 μA-cm (21 nA-m). In [5], an implanted dipole of 16 mm length was stimulated with 4 μA current, for an equivalent 64 nA-m current dipole. We wished to establish a baseline dipole intensity of the proper order of magnitude that was readily scaled to other intensities, and that appeared physically plausible. We selected 10 nA-m as our dipole intensity.

The selection of a standard deviation for the noise is not immediately obvious, in part because of the widespread practice of averaging experimental data. In theory, we could average the trials until the noise is reduced to any arbitrary low value. In this EEG/MEG comparison, the noise standard deviation is in units of either volts or teslas, respectively; thus we cannot easily set a standard deviation general to both sensor types as we did with the dipole intensity.

A dipole of intensity 10 nA-m near the cerebral spinal fluid layer can generate a field that peaks roughly at 350 fT in MEG sensors, or at 4 μV in nearby EEG sensors, for the sensor patterns and model examined in this paper. In research such as that of [7], the standard deviation is expressed as a percentage of the peak, approximately 10 percent. This definition roughly translates into similar SNRs examined in [1], [15], [17]. We therefore, somewhat arbitrarily, set the MEG noise standard deviation to 35 fT and the EEG noise standard deviation to 0.4 μV, to reflect this 10:1 ratio. We compare with [3], who had a stated noise level of 50 fT after averaging 200 trials. We note the difficulty in extracting absolute noise levels from other reports for comparison because of the widespread practice of normalizing the noise standard deviation into the field levels.

4.1 Single Tangential Dipole

In this study, we arranged three rings of sensors, with each spaced in increments of 12 degrees from the z-axis and each containing 6, 12, and 18 sensors, respectively, for a total of 37 sensors, as displayed in Fig. 1. The MEG sensors were oriented radially. This pattern approximates that of commercially available 37-channel MEG instruments.

We calculated the lower bound for a single dipole located anywhere in the positive x-z plane (y = 0). The dipole was stepped along at 1 mm intervals within the brain sphere. At each location, the moment angle was stepped in 1 degree increments from 0 to 179 degrees, and at each angle the RMS lower bound was calculated. The average RMS lower bound was calculated over all 180 degrees, and the best and worst angles were located. At these extrema, either a minimization or a maximization algorithm was initiated to refine the estimate of the best and the worst RMS errors, respectively. Three different bounds were retained for each location point in the grid, representing the best, average, and worst RMS errors.

Fig. 3 and Fig. 4, respectively, show the EEG and MEG case for the single dipole restricted to the tangential plane. The best and worst displays differed primarily at the edges of the array. The overall effect is a relatively small error region directly under the array where the errors would be desirable.

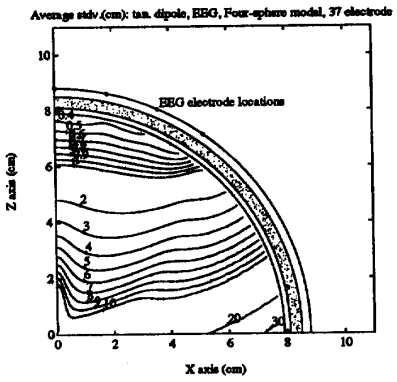

FIGURE 3. Average EEG error lower bound for 37 sensor array, for a single dipole.

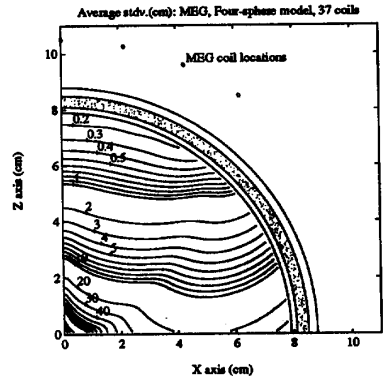

FIGURE 4. Average MEG error lower bound for 37 sensor array, for a single dipole.

4.2 Two Tangential Dipoles

We now examine the rapid degradation in performance that occurs by introducing a second dipole. For simplicity in examining the effect of an additional dipole on the localization accuracy of the original dipole, we fixed the location of the second dipole on the z-axis at z = 7.5 cm, directly under the center of the array. Both dipoles had equal intensity Q, so all results are directly scalable to any other arbitrary intensity. By the symmetry of the location of the additional dipole on the z-axis, we can restrict our analysis region to the positive x-z plane and infer the results for the remainder of the upper hemisphere.

As in the single dipole studies, the first dipole was stepped along on a 1 mm grid within the positive x-z plane. At each location point, the angles of *both* of the dipoles were stepped in 10 degree increments from 0 to 170 degrees, resulting in a grid of 18 by 18 different angle combinations. For each angle pair, the RMS error bounds for the first dipole were calculated as defined by (6). The average errors were then calculated from this two-dimensional

grid of error bounds, and the best and worst angle pairs were found. At these grid point extrema, a Nelder-Meade simplex minimization or maximization algorithm was initiated to refine the estimate of the best or worst RMS error bounds.

Fig. 5 and Fig. 6, respectively, show the best and worst MEG RMS error bounds of a dipole when an additional dipole of equal intensity was placed on the z-axis at z = 7.5 cm. The EEG bounds were not dramatically different in appearance, and space limitations prevent their presentation here. We can see that, in almost all regions, the dipole's error bound is at least double those in the single dipole study. In the worst case, we also found that it is impossible to place two dipoles on the z-axis in the same orientation and still resolve them. This perfect array ambiguity is a consequence of the three perfectly symmetric rings of sensors. The best orientation pair is generally dipoles oriented orthogonal to each other, and the general overall accuracy region is greatly reduced from that of any of the other sensor patterns.

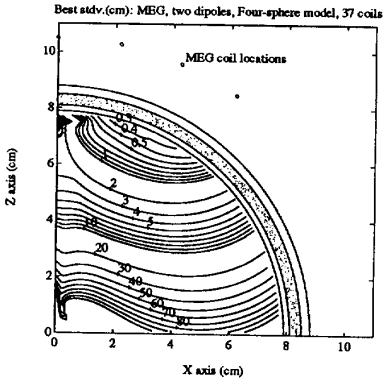

FIGURE 5. Best error lower bound for 37 MEG sensor array, for a one dipole, when a second dipole is fixed at z=7.5cm. EEG results were comparable.

5.0 Monte Carlo Simulation

For each point on a 5 mm grid across the positive quadrant of the x-z plane, we positioned a dipole in the best moment orientation as found by our CRLB analysis. We synthesized the single dipole forward model across the array using the same dipole intensity as in the analysis, then added 100 realizations of zero mean white Gaussian noise at the sensors, using a random number generator with the same standard deviation as that used in the analysis. We then estimated the dipole location parameters for each noise realization using the Nelder-Meade nonlinear least-squares approach described in [10].

From the locations estimated for each of the 100 data sets at each dipole location, we computed the RMS location error for that position. Fig. 7 presents the results, along with the corresponding CRLB analytic results. The overall result is a confirmation of both the MEG CRLB formulas and evidence that the least-squares estimator comes very close to meeting the CRLB.

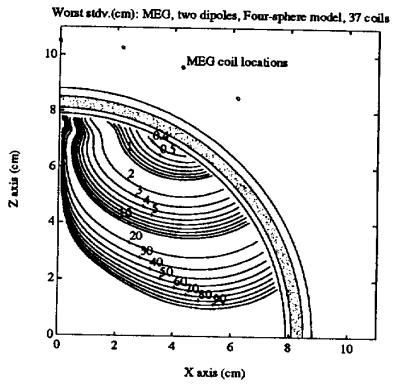

FIGURE 6. Worst error lower bound for 37 MEG sensor array, for one dipole, when a second dipole is fixed at z=7.5cm. EEG results were comparable.

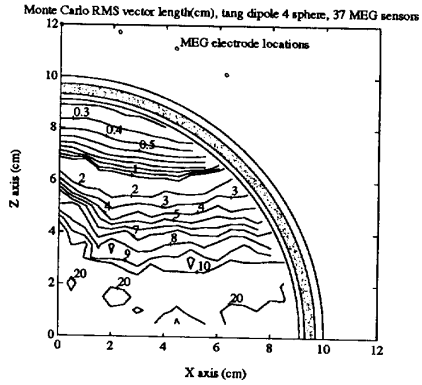

FIGURE 7. Monte Carlo results for 100 trials, at each point on a 5mm grid.

6.0 EEG and MEG Fusion

The field pattern generated by a dipole across an array of EEG sensors roughly peaks along the axis of the dipole moment. In contrast, the MEG pattern peaks to the sides of the dipole moment, roughly perpendicular to the EEG pattern. In this study, we assume that both the EEG and MEG data are acquired, and we observe the improvement generated by this diversity in the information content. The sensor pattern was the same as that in the 37 sensor system, except that here we have a total of 74 measurements for the two combined sensor systems. The analysis procedure was identical to that in the other studies. Unlike the other stud-

ies, the results do *not* scale with arbitrary dipole intensity and noise variance, because both the EEG and MEG noise must be considered simultaneously. To bring the two modalities into relatively scaled units, we multiplied one of the arrays by the ratio of the two noise variances, which introduces a more complex relationship between standard deviation, dipole intensity, and noise variances.

Fig. 8 shows fusion of a dipole restricted to the tangential plane. In the regions directly below the center of the array, an improvement occurs simply because there is twice as many measurement points. In the deeper regions, the EEG sensors have obviously improved the response near the center, and both sensor modalities have greatly improved the other deep regions.

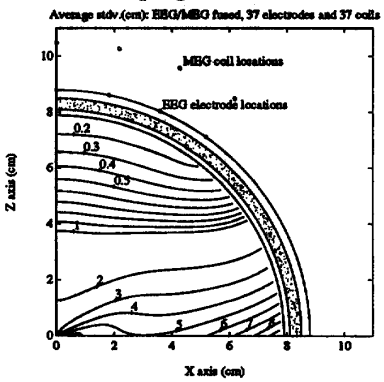

FIGURE 8. Fusion of EEG and MEG measurements.

This analysis confirms the hypotheses of [2], [4], [16] concerning the potential for directly combining EEG and MEG measurements into an overall superior resolution ability, unachievable by either modality alone. One extension of this study would be to augment fixed MEG sensor arrays with a smaller array of EEG sensors to determine whether similar improvements could be obtained.

References

[1] Achim A, Richer F, Saint-Hilaire JM, "Methodological considerations for the evaluation of spatio-temporal source models," *Electroenceph. clin. Neurophysiology.*, 1991, 79: 227 - 240.

[2] Anogianakis G, Badier JM, Barret G, et al. "A consensus statement on relative merits of EEG and MEG," Editorial, *Electroenceph. clin. Neurophysiology.*, 1992, 82: 317 - 319.

[3] Balish M, Sato S, Connaughton P, and Kufta C. "Localization of implanted dipoles by magnetoencephalography," *Neurology* 1991; 41:1072-1076.

[4] Cohen D, and Cuffin BN, "Demonstrations of useful differences between magnetoencephalogram and electroencephalogram," *Electroenceph. clin. Neurophysiol.* 1983, 56:38-51.

[5] Cohen D, Cuffin BN, Yunokuchi K, Maniewski R, Purcell C. Cosgrove GR, Ives J, Kennedy JG, Schomer DL. "MEG versus EEG localization test using implanted sources in the human brain," *Ann Neurol* 1990, 28:811-817.

[6] Cuffin BN, Cohen D, "Comparison of the magnetoencephalogram and electroencephalogram," *Electroenceph. clin. Neurophysiol.*,1979, 132-146.

[7] Cuffin BN, "Effects of measurement errors and noise on MEG moving dipole inverse solutions," *IEEE Trans. Biomedical Eng.*, 1986, 33: 854 - 861.

[8] Hari, R., Hamalainen M, Ilmoniemi, R. Lounasmaa, OV. "MEG versus EEG localization test," Letter to the Editor, *Ann Neruol.* 1991, 30: 222-223.

[9] Mosher JC, Lewis PS, Leahy RM, "Spatial localization of neural sources using the magnetoencephalogram," *Fifth ASSP Wkshp on Spectrum Estimation and Modeling*, Rochester, NY, Oct 1990:289-293.

[10] Mosher JC, Lewis PS, and Leahy RM, "Multiple dipole modeling and localization from spatio-temporal MEG data," *IEEE Trans. Biomedical Eng*, 1992, 39:541-557.

[11] Mosher JC, Spencer ME, Leahy RM, and Lewis PS, "Error bounds for EEG and MEG dipole source localization," *Electroencephalography and clinical Neurophysiology* (in press) 1992.

[12] Sarvas J, "Basic mathematical and electromagnetic concepts of the biomagnetic inverse problem," *Phys. Med. Biol.*, 1987, 32:11-22.

[13] Spencer ME, Leahy RM, Mosher JC, and Lewis PS, "Adaptive filters for monitoring localized brain activity from surface potential time series," *IEEE Proc. 26th Asilomar Conf. on Signals, Systems, and Computers*, Pacific Grove, CA, Oct. 1992 (this volume).

[14] Stoica P, and Nehorai A, "MUSIC, maximum likelihood, and Cramer-Rao Bound," *IEEE Transactions on Acoustics, Speech, and Signal Processing*, 1989, 37:720-741.

[15] Stok CJ, "The influence of model parameters on EEG/MEG single dipole source estimation," *IEEE Trans. Biomedical Eng.*, 1987, 34: 289 - 296.

[16] Therapeutics and Technology Assessment Subcommittee, "Assessment: Magnetoencephalography (MEG)," *Neurology* 1992; 42: 1-4.

[17] Westerkamp JJ, Aunon JI. "Optimum multielectrode a posteriori estimates of single-response evoked potentials," *IEEE Trans. Biomedical Eng.*, 1987, 34: 13 - 22.

[18] Williamson, SJ "MEG versus EEG localization test," Letter to the Editor, *Ann Neruol.* 1991, 30: 222.